Bioactive Materials 28 (2023) 326–336

Contents lists available at ScienceDirect

Bioactive Materials

journal homepage: www.keaipublishing.com/en/journals/bioactive-materials

Cryo-shocked cancer cell microgels for tumor postoperative combination immunotherapy and tissue regeneration

Gaizhen Kuang [a,c], Qingfei Zhang [c], Yunru Yu [c], Luoran Shang [b,**], Yuanjin Zhao [a,c,*]

[a] Department of Rheumatology and Immunology, Nanjing Drum Tower Hospital, School of Biological Science and Medical Engineering, Southeast University, Nanjing, 210096, China
[b] Shanghai Xuhui Central Hospital, Zhongshan-Xuhui Hospital, and the Shanghai Key Laboratory of Medical Epigenetics, The International Co-laboratory of Medical Epigenetics and Metabolism (Ministry of Science and Technology), Institutes of Biomedical Sciences, Fudan University, Shanghai, 200032, China
[c] Oujiang Laboratory (Zhejiang Lab for Regenerative Medicine, Vision and Brain Health), Wenzhou Institute, University of Chinese Academy of Sciences, Wenzhou, Zhejiang, 325001, China

ARTICLE INFO

Keywords:
Immunotherapy
Microfluidics
Microgel
Vaccine
Regeneration

ABSTRACT

Prevention of recurrence/metastasis and tissue regeneration are critical for post-surgery treatment of malignant tumors. Here, to address these needs, a novel type of microgel co-loading cryo-shocked cancer cells, immunoadjuvant, and immune checkpoint inhibitor is presented by microfluidic electrospray technology and liquid nitrogen treatment. Owing to the encapsulation of cryo-shocked cancer cells and immunoadjuvant, the microgels can recruit dendritic cells and activate them *in situ*, and evoke a robust immune response. Moreover, with the combination of the immune checkpoint inhibitor, the antitumor immune response is further enhanced by inhibiting the interaction of PD1 and PDL1. With this, the excellent anti-recurrence and anti-metastasis efficacy of the microgels are demonstrated in an orthotopic breast cancer mouse model. Besides, because of the excellent biocompatibility and appropriate degradation performance, the microgels can provide support for normal cell adhesion and growth, which is beneficial to tissue reconstruction. These properties indicate the great value of the cryo-shocked cancer cell microgels for efficient tumor postoperative combination immunotherapy and tissue regeneration.

1. Introduction

Cancer is among the diseases with the highest fatality rate worldwide, and surgery is still the preferred treatment for most malignant solid tumors in clinics [1]. Unfortunately, tumor recurrence and metastasis rates are still high after surgery resection, which seriously threatens the survival of the patients [2,3]. Traditional post-surgery treatments, such as chemotherapy and radiotherapy, face the problems of severe side effects and limited efficacy [4–10]. Alternatively, immunotherapy is an emerging strategy that brings new solutions to cancer treatment [11]. However, the repeated and systemic injection of immunotherapy agents, including dendritic cell (DC) vaccine, immune checkpoint inhibitors, adoptive T cells, cytokines, etc., may result in uncontrolled immune responses and adverse events [12–15]. To improve immunotherapy efficacy and reduce side effects, synthetic scaffold materials have been employed to regulate the tumor microenvironment as well as achieve the loading, localization, and delivery of the bioactive agents [16–18]. Although with much progress, there remains the dilemma of insufficient interaction between immune cells and scaffolds and limited immune activation [19,20]. In addition, the regeneration of postoperative tissue defects is an important factor that affects the life quality of patients, while the existing immunotherapy scaffolds barely contribute to this [21,22]. Therefore, novel multifunctional immunologic therapeutic systems for tumor postoperative treatment and reconstruction are highly anticipated.

In this paper, we proposed cryo-shocked cancer cell-loaded microgels for combination immunotherapy and tissue regeneration, as schemed in Fig. 1. Cryo-shocked cancer cells are inactivated cells

Peer review under responsibility of KeAi Communications Co., Ltd.
* Corresponding author. Department of Rheumatology and Immunology, Nanjing Drum Tower Hospital, School of Biological Science and Medical Engineering, Southeast University, Nanjing, 210096, China.
** Corresponding author.
E-mail addresses: luoranshang@fudan.edu.cn (L. Shang), yjzhao@seu.edu.cn (Y. Zhao).

https://doi.org/10.1016/j.bioactmat.2023.05.021
Received 2 March 2023; Received in revised form 8 May 2023; Accepted 30 May 2023
2452-199X/© 2023 The Authors. Publishing services by Elsevier B.V. on behalf of KeAi Communications Co. Ltd. This is an open access article under the CC BY-NC-ND license (http://creativecommons.org/licenses/by-nc-nd/4.0/).

generated by freezing [23]. It has been demonstrated that cryo-shocked cancer cells can act as cancer vaccines and provoke the antitumor immune response [24]. Besides, microfluidics is an outstanding technology capable of manipulating multiple fluids in microchannels, and has been extensively utilized for the preparation of diverse microparticles [25–27]. These microparticles serve as vehicles for the encapsulation and delivery of small-molecule drugs, biomacromolecules, and even cells [28–32]. Particularly, the tunable microstructure of the microparticles provides a superior environment for the contact and interaction of encapsulated agents with the surroundings compared with bulk systems [33]. Moreover, by introducing biocompatible materials like gelatin, hyaluronic acid, etc., the resultant microgels can be promising in tissue regeneration due to their similarity with the natural extracellular matrix (ECM) [34–36]. It was thus conceived that by constructing cryo-shocked cancer cell-loaded microgels through the microfluidic encapsulation technique, novel functional platforms could be developed for efficient tumor postoperative treatment.

Here, we presented the desired microgels co-loading cancer vaccine and immune checkpoint inhibitor for postoperative combination immunotherapy and tissue regeneration (Fig. 1). Droplets of methacrylate gelatin/methacrylate hyaluronic acid (GelMA/HAMA) were generated by microfluidic electrospray, with cancer cells, cytosine-guanosine oligonucleotide (CpG ODN, an immunoadjuvant) and anti-programmed death receptor 1 antibody (aPD1, an immune checkpoint inhibitor) encapsulated. The droplets were collected in liquid nitrogen and crosslinked *in situ* via ultraviolet (UV) polymerization. With this, the encapsulated cancer cells were cryo-inactivated to act as whole-cell tumor antigens. Additionally, the cryo-shocked cancer cells, together with the CpG ODN, can recruit and activate DCs both *in vitro* and *in vivo*, thus provoking a strong immune response. Apart from these, the existence of aPD1 could enhance the antitumor immune response by inhibiting the interaction of PD1 and programmed cell death ligand 1 (PD-L1). By applying the resultant microgels in a breast cancer mouse model, their excellent anti-recurrence and anti-metastases efficiency was demonstrated. Moreover, the double network of GelMA/HAMA imparted the microgels with sufficient physical support and slow degradation performance, which was beneficial for cell adhesion and growth for tissue reconstruction. These features indicated that the cryo-shocked cancer cell microgels have significant potential as a versatile system for postoperative combination immunotherapy and tissue reconstruction.

2. Materials and methods

2.1. Materials

GelMA and HAMA were synthesized in our laboratory. Bouin's solution was obtained from Fuzhou Phygene Biotechnology Co., LTD. Carboxyfluorescein diacetate succinimidyl ester (CFDA SE) cell proliferation assay and tracking kit, red blood cell lysis buffer, collagenase I, collagenase II, collagenase IV, hyaluronidase, cell counting kit 8 (CCK8), and Calcein AM/PI Live/Dead viability assay kit were bought from Shanghai Beyotime Biotechnology Co., Ltd. 1′-dioctadecyltetramethyl indotricarbocyanine Iodide (DiR) was bought from Beijing Lablead Trading Co., LTD. Mouse TNF-α, mouse IL-6, and rat IgG ELISA kits were provided by Wuhan Elabscience Biotechnology Co., Ltd. aPD-1 (rat anti-mouse) and antibodies for flow cytometry used in this study were purchased from Biolegend Inc. (USA). Lithium phenyl-2,4,6-trimethylbenzoylphosphinate (LAP) was obtained from Shanghai Aladdin Co., Ltd. CpG ODN 1826, with the sequence 5′-tccatgacgttcctgacgtt-3′ and a phosphorothioate backbone, and CPG ODN 1826 labeling with FAM on 3′ end (named FAM-CpG ODN) were obtained from

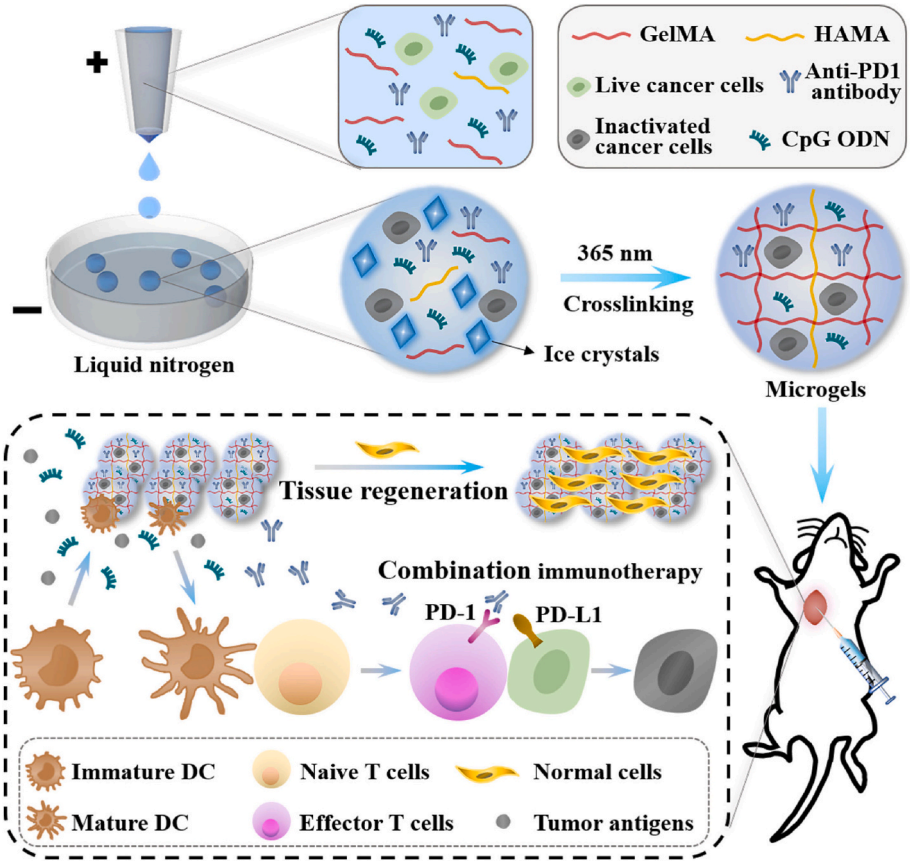

Fig. 1. Schematic illustration of the preparation of cryo-shocked cancer cell microgels and their application in tumor postoperative combination immunotherapy and tissue regeneration.

Suzhou Synbio Technologies Co.

2.2. Preparation of the microgels

PBS solution containing GelMA (10% w/v), HAMA (1% w/v), immunoadjuvant CpG ODN (500 μg/mL), mouse breast cancer 4T1 cells (1.0×10^7/mL), aPD-1 (750 μg/mL) and photoinitiator LAP (4 mg/mL) was stirred at 37 °C to ensure full dissolution. The resultant solution was dispensed into liquid nitrogen by a microfluidic electrospray device, and then photo-crosslinked under 365 nm irradiation. The voltage was 3.3 Kv, the tip diameter was 100 μm, and the distance between the jet and collector was 8 cm. The obtained microgels containing CpG ODN, 4T1 cells, and aPD-1 were named MG-V+A. Microgels without the above components (named MG-Blank), microgels containing adjuvant CpG ODN (named MG-Adjuvant), microgels containing cryo-shocked cancer cells (named MG-Cells), microgels containing CpG ODN and cryo-shocked cancer cells (named MG-Vaccine), and microgels containing aPD-1 (named MG-aPD1) were prepared with the same parameters.

2.3. Characterization of the microgels

MG-Blank and MG-V+A were dispersed in PBS. The morphologies of the microgels were observed by optical microscope and their diameters were analyzed. The supercritical dried MG-Blank and MG-V+A, and the cross-section of the freeze-dried microgels were observed via field emission scanning electron microscopy (SEM, SU8010, Hitachi, Japan). MG-V+A were digested by collagenase II and hyaluronidase, and the obtained cancer cells were counted under an optical microscope.

2.4. In vitro release of CpG ODN and aPD1

The cryo-shocked cancer cell microgels with FAM-CpG ODN were placed in PBS at 37 °C and 120 rpm. At every time interval, a certain volume of release medium was removed and the fresh medium with the same volume was added. The amount of FAM–CpG ODN released into the media was determined by the intensity of FAM fluorescence in the supernatant using a full wavelength microplate reader (Varioskan LUX, ThermoFisher, American) with 492 nm ex/517 nm em, calibrated by a serial dilution of FAM–CpG ODN standard solutions. MG-V+A was used to investigate the release profiles as described above and the aPD1 concentrations were quantified by Rat IgG total ELISA kit. The cryo-shocked cancer cell microgels with FAM-CpG ODN or MG-V+A were digested by collagenase II and hyaluronidase, and the contents of CpG ODN and aPD1 were measured by full wavelength microplate reader and Rat IgG total ELISA kit, respectively.

2.5. In vivo fluorescence imaging of microgels

200 μL cryo-shocked cancer cell microgels containing 4T1 cells labeled with DiR were injected subcutaneously into female BALB/c mice through a syringe. At the preset points in time, the mice were anesthetized and imaged using a multi-mode *in vivo* imaging system (IVIS Lumina XRMS Series III, PerkinElmer, American) with 710 nm ex/760 nm em.

2.6. In vitro biocompatibility study

200 μL MG-V+A was soaked in the culture medium for 24 h. The leaching solution was diluted to different concentrations. Mouse fibroblasts NIH 3T3 cells were cultured with these diluted microgel leaching solutions for 24 h or 48 h, and CCK8 assay was used to test the cell viability.

2.7. In vivo degradation test

200 μL MG-V+A was injected subcutaneously into female BALB/c mice through a syringe. The injected samples were harvested on days 7, 14, 28, and 56. By weighing the dry weight of the samples, the remaining mass percentages were calculated.

2.8. In vitro recruitment of DCs

Bone marrow-derived dendritic cells (BMDCs) were isolated from the mice and labeled with CFDA SE according to the relevant guidance. Transwell plates (24-well, 8 μm pore filters, Corning Inc., American) were used to study DC recruitment. The upper compartment was seeded with CFDA SE-labeled BMDCs. The lower compartment was placed with medium and 50 μL MG-Blank of, MG-Adjuvant, MG-Cells, or MG-Vaccine. After 24 h, the cells migrating from the upper compartment into the lower compartment were visualized and counted by fluorescence microscope.

2.9. In vitro activation of DCs

BMDCs were incubated with 50 μL MG-Blank, MG-Adjuvant, MG-Cells, or MG-Vaccine for 24 h. The collected cells were stained with FITC-anti-CD11c, PE-anti-CD80, and APC-anti-CD86, and were analyzed with a flow cytometer (CytoFLEX, Beckman Coulter, German). The supernatants were used to detect TNF-α and IL-6 secretions via ELISA kits.

2.10. In vivo immunization

MG-Blank or MG-Vaccine of 200 μL was injected into the mice subcutaneously. Microgels, lymph nodes (LNs), and spleens were excised 7 days after implantation. The microgels were digested with collagenase I (500 μg/mL), collagenase IV (100 μg/mL), and hyaluronidase (100 μg/mL) at 37 °C for 1 h and then filtered using a 40 μm Falcon cell strainer to prepare single cells, which were further blocked with anti-mouse CD16/32. The cells were stained with FITC-anti-CD11c, PE-anti-CD80, and APC-anti-CD86 simultaneously. Spleens and LNs were homogenized using frosted slides to prepare single cells, which were further blocked with anti-mouse CD16/32. The cells from LNs were stained with FITC-anti-CD11c, PE-anti-CD80, and APC-anti-CD86 simultaneously, or FITC-anti-CD3, APC-anti-CD4, and PE-anti-CD8a simultaneously, and the cells from spleens were stained with FITC-anti-CD3, APC-anti-CD4, and PE-anti-CD8a simultaneously. The stained cells were analyzed with a flow cytometer.

2.11. Fluorescence imaging of the microgels in vivo and draining LNs ex vivo

200 μL MG-Vaccine containing 4T1 cells labeled with CFDA SE was injected into the mice subcutaneously and the mice were imaged using a multi-mode *in vivo* imaging system. 7 days after the injection, draining LNs were excised and imaged using a multi-mode *in vivo* imaging system.

2.12. In vivo anti-recurrence and anti-metastases experiment

To establish the orthotopic breast tumor model, 100 μL 4T1 cells (1×10^7 cells/mL) were injected into the right mammary fat pads of mice. When the volume of the tumors reached about 100 mm^3, the mice were anesthetized. Ophthalmic scissors were used to separate the skin at the tumor site and the tumor was exposed. After complete removal of the visible tumor, 200 μL MG-Blank, MG-Vaccine, MG-aPD-1, or MG-V+A were immediately injected into the surgery region and then the incision was sutured. The mice without microgels were set as control. According to the treatments, the mice were grouped as follows ($n = 5$): Control group, MG-Blank group, MG-Vaccine group, MG-aPD-1 group, and MG-V+A group. 14 days after the operation, both tumors and lungs were collected and photographed. The tumors were weighted. Then the tumors were fixed in 4% paraformaldehyde and tested by hematoxylin and eosin (H&E) staining and with a TdT-mediated dUTP Nick-End Labeling

(TUNEL) apoptosis detection kit. After being fixed in Bouin's solution, the numbers of white metastasis nodules macroscopically in the lung tissues were counted. Histological alterations were also assessed by H&E staining.

To evaluate the survival of mice, another set of mice with the same grouping and the same sample number as above were monitored and euthanized for humane reasons when the longest axis of the tumor reached 15 mm.

2.13. Anti-tumor mechanism

When the tumor volumes reached about 100 mm^3, 50% of the tumor tissues were resected, and 200 μL corresponding microgels were injected directly into the surgery region. 7 days after the operation, the mice were sacrificed. The harvested tumors were digested with collagenase I, collagenase IV, and hyaluronidase to prepare single cells. After being blocked with anti-mouse CD16/32, some of the cells were stained with FITC-anti-CD3 and PE-anti-CD8a simultaneously and others were stained with FITC-anti-CD3 and APC-anti-CD4, and then with PE-anti-FoxP3. The stained cells were analyzed with a flow cytometer.

2.14. In vitro cell attachment property

50 μL MG-Blank was cultured with human breast epithelial cells MCF-10A or human adipose-derived stem cells ADSCs (1×10^5 cells/mL). After 24 h, the obtained microgels were fixed by 4% paraformaldehyde, and then dehydrated by gradient ethyl alcohol and supercritical drying. The morphology of cell-attached microgels was characterized via SEM.

2.15. In vitro cell proliferation property

After co-culture of MCF-10A or ADSCs with MG-Blank for 24 h, the microgels were placed in the fresh culture medium. After culture for 1, 2, and 4 days, the viability of cells adhered to the microgels was tested by CCK8 assay. Calcein-AM staining was used to observe cell growth conditions, and the images were obtained by fluorescence microscope.

2.16. In vivo tissue regeneration

200 μL MG-Blank was injected subcutaneously into the mice. The injected samples were harvested on days 0, 7, and 21. The obtained microgels were fixed in 4% paraformaldehyde and tested by H&E staining.

2.17. Statistical analysis

All values are presented as mean ± standard deviation (SD). Statistical analysis was evaluated using GraphPad Prism. The significance of differences between the two groups was calculated by a two-tailed unpaired Student's *t*-test. The significance of differences between more than two groups was analyzed by one-way ANOVA using the Turkey post-hoc test. For animal survival, the significance of differences was determined by log-rank test. $P < 0.05$ was considered significant.

3. Results and discussion

3.1. Preparation and characterization of microgels

As synthetic polymers originated from gelatin and hyaluronic acid, GelMA and HAMA are chosen to prepare the desired microgels. In a typical experiment, GelMA/HAMA droplets were first formed by microfluidic electrospray and collected in liquid nitrogen, after which they were crosslinked under UV radiation to obtain GelMA/HAMA microgels (MG-Blank). As shown in Figs. S1 and S2, MG-Blank exhibited well-dispersed size distribution with a mean diameter of 235 μm. SEM images displayed the wrinkled surface structure and the porous interior structure of MG-Blank (Fig. S3). These results demonstrated the successful fabrication of the photo-crosslinkable microgels by microfluidic electrospray without the use of oil or organic solvent. Besides, the cell viability and proliferative activity of liquid nitrogen-treated cells were evaluated. We found that the cancer cells treated with liquid nitrogen were inactivated, as manifested by the fluorescent live/dead assay results shown in Fig. S4. Compared with the gradually elevated absorbance of live cells, the absorbance of the liquid nitrogen-treated cancer cells kept at a constant level, indicating the loss of the proliferative ability of the tumor cells treated by liquid nitrogen (Fig. S5).

UV radiation with appropriate intensity and time has little impact on the active components including proteins, nucleic acids, and even live cells [37–39]. Based on this, we prepared cryo-shocked cancer cell-loaded microgels by electrospraying a GelMA/HAMA solution containing cancer cells, CpG ODN, and aPD1 into liquid nitrogen and then polymerizing the droplets with UV. Compared with MG-Blank generated under the same experimental parameters, the microgels co-loaded with vaccine and aPD1 (MG-V+A) showed little difference in mean diameter (236 μm) and morphology (Fig. 2a, **2b**, and Fig. S6). The obtained microgels maintained the porous structure and cancer cells could be observed, indicating the successful encapsulation (Fig. 2bii, **2biii**) and Fig. S3ii, **S3iii)).** Furthermore, the cryo-shocked cancer cell microgels were digested by collagenase II and hyaluronidase for quantifying cancer cells, CpG ODN, and aPD1. There were ~1.6×10^6 inactivated 4T1 cells, 61.5 μg CpG ODN, and 101.7 μg aPD1 per 200 μL MG-V+A. The release profiles of CpG ODN and aPD1 were tested by spectrofluorimetry and ELISA, respectively. As shown in Fig. 2c and **d**, FAM-CpG ODN exhibited a relatively quick burst release of 68.72% on the first day and then a slower release till the seventh day when the release process was completed; aPD1 was released in a sustained manner to approximately 20 days. In order to investigate the change of the inactivated cancer cells encapsulated in the microgels, DiR was used to label cancer cells and then the obtained cells were applied to prepare microgels for *in vivo* fluorescence. As shown in Fig. S7, the fluorescence intensity in the injection site gradually decreased, indicating the decomposition of the cancer cells. Owning to the action of immune cells and enzymes *in vivo*, the inactivated cancer cells were disintegrated and the tumor antigens were subsequently released gradually. These results demonstrated the successful preparation of the cryo-shocked cancer cell-loaded microgels and the sustained release of the encapsulated therapeutic components.

As a material for implant use, biocompatibility and biodegradation are important factors for the microgels serving as both tissue regeneration scaffold and drug delivery system. The leaching solution of MG-V+A was co-cultured with mouse fibroblasts NIH 3T3 cells. The results of the CCK8 assay showed that MG-V+A had no obvious cytotoxicity to 3T3 cells with the increase of the leaching solution concentration and co-culture time, indicating good biocompatibility (Fig. 2e and Fig. S8). Then the *in vivo* degradation behavior of MG-V+A was investigated by subcutaneous injection. As shown in Fig. 2f, the microgels formed a round-like nodule subcutaneously. No significant change of the nodule morphology was observed for up to 4 weeks, indicating the local retention of the microgels, which is favorable for long-term and stable cell adhesion. In the first week, the mass of the injected microgels increased, which might be attributed to the adsorption of body fluid and the infiltration of cells (Fig. S9). Then, the mass gradually decreased with the degradation of the microgels, and the nodule still existed in week 8. These results indicated that the cryo-shocked cancer cell-loaded microgels possessed good biocompatibility and an appropriate biodegradation rate.

3.2. In vitro DC recruitment and maturation

Sufficient DC recruitment and maturation of DCs are of great importance for the microgels to activate the immune response.

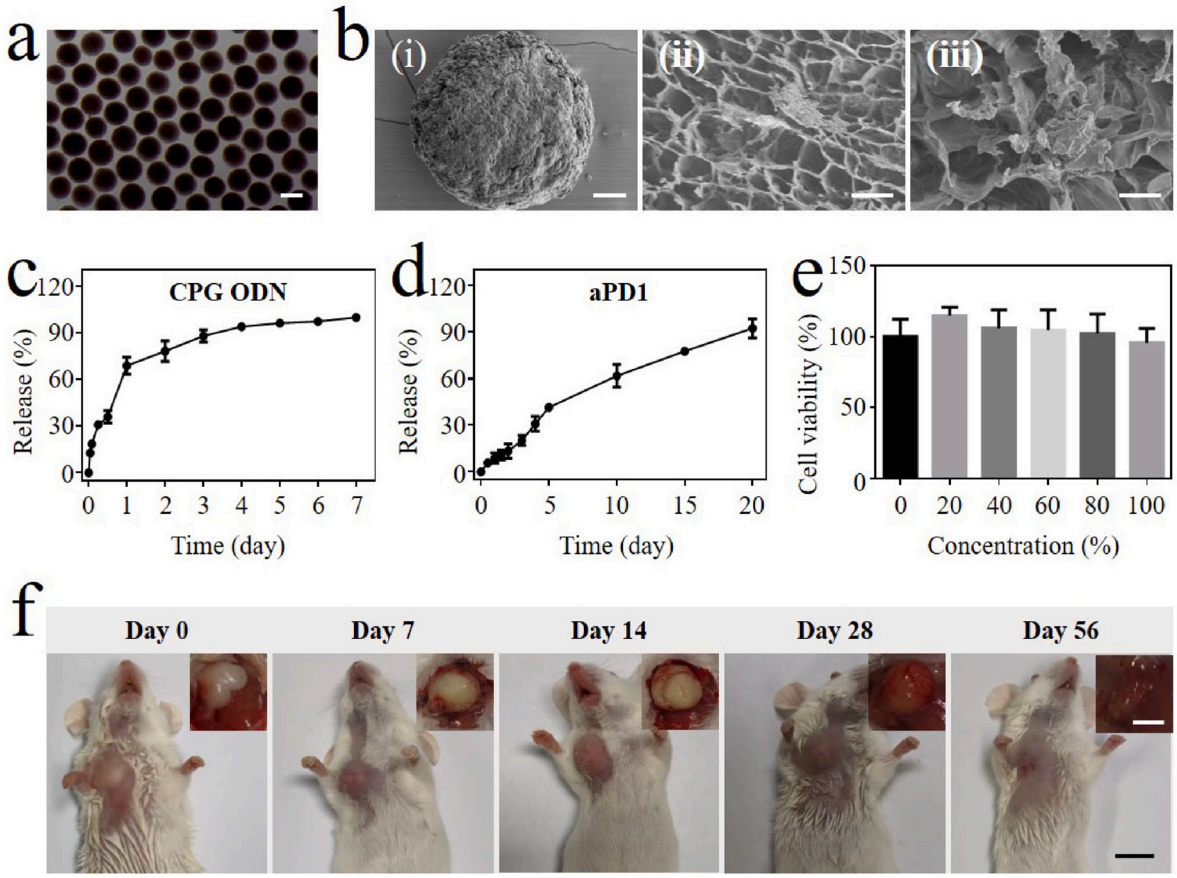

Fig. 2. Characterization of the cryo-shocked cancer cell microgels. (a) Optimal image of the microgels. Scale bar is 200 μm. (b) SEM images of (i) an entire microgel and (ii, iii) its cross-section. Scale bars are 20 μm in (i), 10 μm in (ii) and 5 μm in (iii). (c) Release profile of CPG ODN (n = 3). (d) Release profile of aPD1 (n = 3). (e) 3T3 cell viability co-cultured with the leaching solution of the microgels for 24 h (n = 5). (f) Images of the mice and the separated microgels (insert) on different days after injection of 200 μL cryo-shocked cancer cell microgels. Scale bars are 1 cm in the main images and 0.5 cm in the insert images. Data are presented as mean ± SD.

Transwell cell migration assay was used to determine the capability of the microgels in recruiting DCs. Microgels encapsulated with immunoadjuvant (MG-Adjuvant), cryo-shocked tumor cells (MG-Cells), both of them (MG-Vaccine), or none of them (MG-Blank) were prepared and located in the lower compartment, while BMDCs stained with CFDA SE were placed in the upper compartment. After 24 h, the BMDCs migrating toward the lower compartment were observed and counted by fluorescence microscope. Compared with the control group (without treatment) and MG-Blank group, more DCs appeared in the lower compartment in the MG-Adjuvant group and MG-Cells group, and this difference was even more pronounced in the MG-Vaccine group (Fig. 3a). The counting results also indicated that the microgels in the MG-Vaccine group recruited the largest amount of DCs among these groups (Fig. 3c). It is thus concluded that tumor antigens (i.e. cryo-shocked cancer cells) and immunoadjuvant (i.e. CpG ODN) encapsulated in the microgels could robustly promote DC recruitment. CpG ODN sequences are a common danger signal which can provoke DC activation and trafficking [40,41]. The chemotaxis of BMDCs in response to antigens will be enhanced by the combination of danger signals [42].

To explore the ability of promoting DC maturation of the microgels, flow cytometry and ELISA were carried out after BMDCs were treated with different stimulation for 24 h. As the markers of DC maturation, CD80 and CD86 expression levels were studied. As shown in Fig. 3b and **d**, the percentage of $CD80^{+}CD86^{+}$ BMDCs was higher in both the MG-Adjuvant group (30.42%) and MG-Cells group (41.14%), and was the highest in the MG-Vaccine group (55.99%), compared with the control group (16.75%) and MG-Blank group (16.28%). The highest expression of CD80 and CD86 in the MG-Vaccine group indicated the strong capability of promoting DC activation. Besides, the cytokines related to DC maturation were also detected. As expected, the secreted TNF-α and IL-6 by BMDCs displayed the same trends as the results of flow cytometry (Fig. 3e and Fig. S10). Consequently, it was concluded that the microgels co-loading cryo-shocked tumor cells and immunoadjuvant were able to potently activate DCs and facilitate the maturation of DCs.

3.3. *In vivo immune response of the microgels*

After confirming that MG-Vaccine could recruit and activate DC *in vitro*, the immunization of the microgels *in vivo* was then investigated. MG-Vaccine or MG-Blank was injected into mice subcutaneously, and the microgels and the draining lymph nodes were separated on day 7 after injection. DCs recruited in the microgels were analyzed. The number of DCs in the MG-Vaccine group was 3.3 times that in the MG-Blank group (Fig. 4b). The CD80 and CD86 surface marker expression of DCs in the MG-Vaccine group was 51.40%, which was higher than that in the MG-Blank group (29.69%) (Fig. 4a and **c**). These results indicated that the microgels co-loading cryo-shocked tumor cells and immunoadjuvant were able to efficiently recruit and activate DCs *in vivo*. Commonly, after the uptake of antigens, immature DCs can differentiate into mature DCs. Then, mature DC migrates from antigen-exposed peripheral tissues into secondary lymphoid organs, where they present antigens to T cells and stimulate an immune response. As a cell tracing probe, CFDA SE can be decomposed into CFSE after being catalyzed by intracellular esterase, and CFSE can bind to lysine residues or other amino groups of intracellular proteins and thus label these proteins. Therefore, MG-Vaccine with cancer cells labeled with CFDA SE was

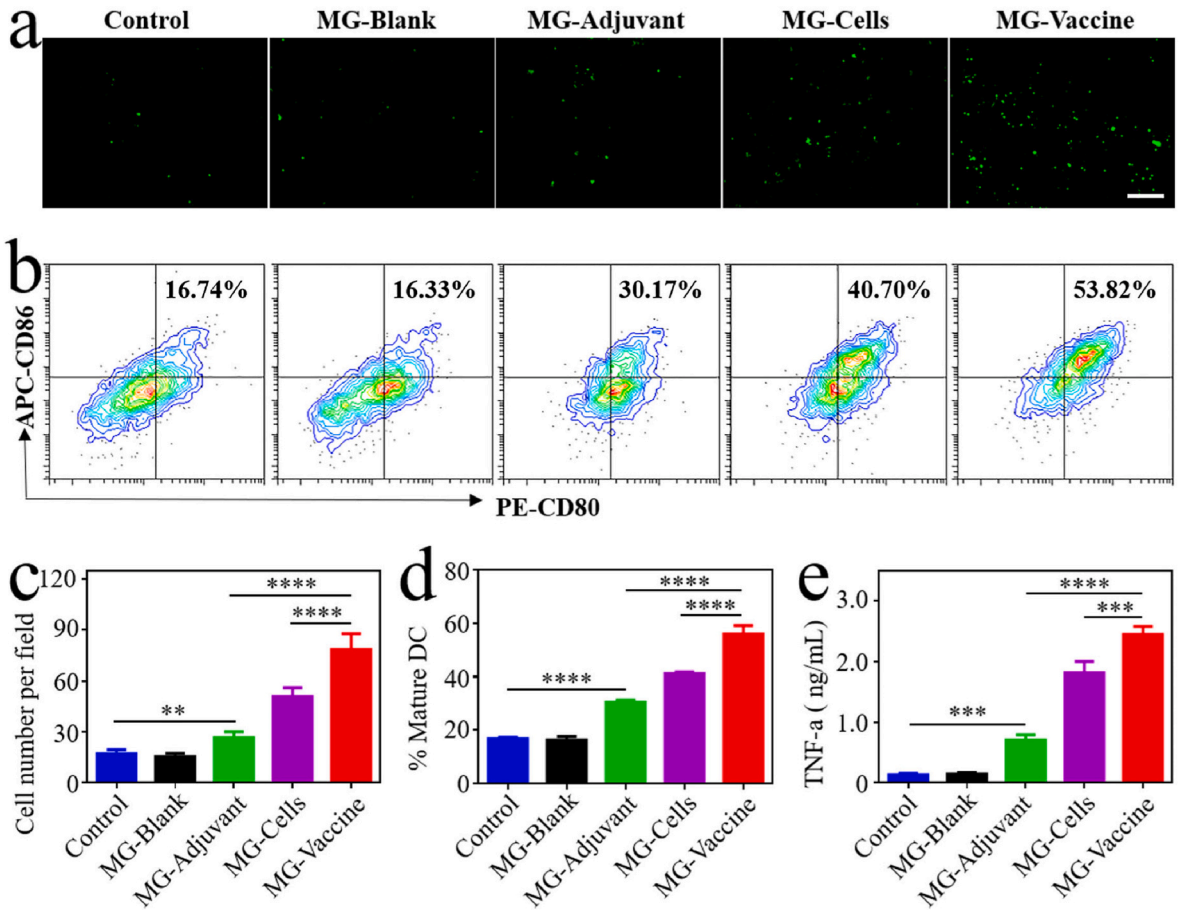

Fig. 3. *In vitro* DC recruitment and maturation induced by the microgels. (a, c) (a) Fluorescence images and (c) counting results of CFDA SE-stained BMDCs by Transwell cell migration assay (n = 3). Scale bar is 200 μm. (b, d) (b) Representative flow cytometry data and (d) statistical data of mature BMDCs with different stimulation for 24 h (n = 3). (e) TNF-α secreted by BMDCs with different stimulation for 24 h (n = 3). Data are presented as mean ± SD. Statistical significance was calculated by one-way ANOVA using the Turkey post-hoc test. *p < 0.05, **p < 0.01, ***p < 0.00, ****p < 0.0001.

injected into the mice subcutaneously to observe the migration of DCs to draining LNs. As shown in Fig. S11, the presence of antigens was visualized by fluorescence imaging at the injection site. 7 days after injection, obvious fluorescence in the LNs isolated from the mice with MG-Vaccine treatment could be seen compared with that of the normal mice, indicating the uptake and transportation of antigens by DCs from the injection site to LNs. Besides, the MG-Vaccine group showed an elevated proportion of $CD80^+CD86^+$ cells in $CD11c^+$ cells (33.46% vs 13.98%) (Fig. S12), also suggesting the extensive migration of the activated DCs from the microgels to LNs. These results provided *in* vivo evidence that MG-Vaccine can efficiently recruit DCs, activate DCs, and promote matured DCs homing to LNs.

Lymph nodes and spleens were separated on day 7 after implantation to detect T cells. As shown in Fig. 4d, **e**, **4g**, and **4h**, the population of $CD8^+$ T cells in both lymph nodes (22.52%) and spleens (12.93%) of mice treated with MG-Vaccine were much higher than that of mice in the MG-Blank group (15.20% and 7.05%, respectively). The higher level of $CD4^+$ T cells in the MG-Vaccine group was also observed in both lymph nodes (46.19% vs 31.04%) and spleens (15.67% vs 10.26%) (Fig. 4f, **i**, and Fig. S13, **S14**), indicating the robust T cell response induced by the MG-Vaccine. Furthermore, lymph nodes and spleens from the MG-Vaccine group were both visibly larger than that from the MG-Blank group (Fig. S15 and Fig. S16), which indirectly validated the immune response initiation in the mice.

3.4. *In vivo antitumor efficacy and mechanism*

A mouse orthotopic breast cancer model was established to investigate the anti-recurrence and anti-metastasis efficacy of the cryo-shocked cancer cell microgels (Fig. 5a). As shown in Fig. S17, when the tumor volume reached ~100 mm^3, an operation was conducted to remove visible tumors to simulate complete tumor resection in clinical practice. The mice were grouped as follows: Control group (without treatment), MG-Blank group (treated with blank microgels), MG-Vaccine group (treated with microgels encapsulating cryo-shocked cancer cells and CpG ODN), MG-aPD1 group (treated with microgels encapsulating aPD1) and MG-V+A group (treated with microgels encapsulating cryo-shocked cancer cells, CpG ODN, and aPD1). Corresponding microgels were injected into the surgery region and then the wounds were sutured.

On day 14 after the operation, recurrent tumors and lung tissues were harvested to evaluate the antitumor efficacy. Due to the presence of residual tumor cells in the surgery region, postoperative tumor recurrence happens. All mice in the Control group, MG-blank group, and MG-vaccine group displayed tumor recurrence. MG-aPD1 group had one mouse without local relapse, while the MG-V+A group had two mice free of recurrence (Fig. 5b). Comparing the weight of the recurrent tumors, the MG-V+A group also showed the best anti-recurrence efficiency (Fig. 5d). H&E staining and TUNEL assay of tumor tissues demonstrated the enhanced necrosis and apoptosis of tumor cells in the MG-V+A group (Fig. S18). Besides, the MG-V+A group showed remarkable anti-metastasis efficiency, as evidenced by the decreased number of metastasis nodules in the lung tissues (Fig. 5c and **e**). The

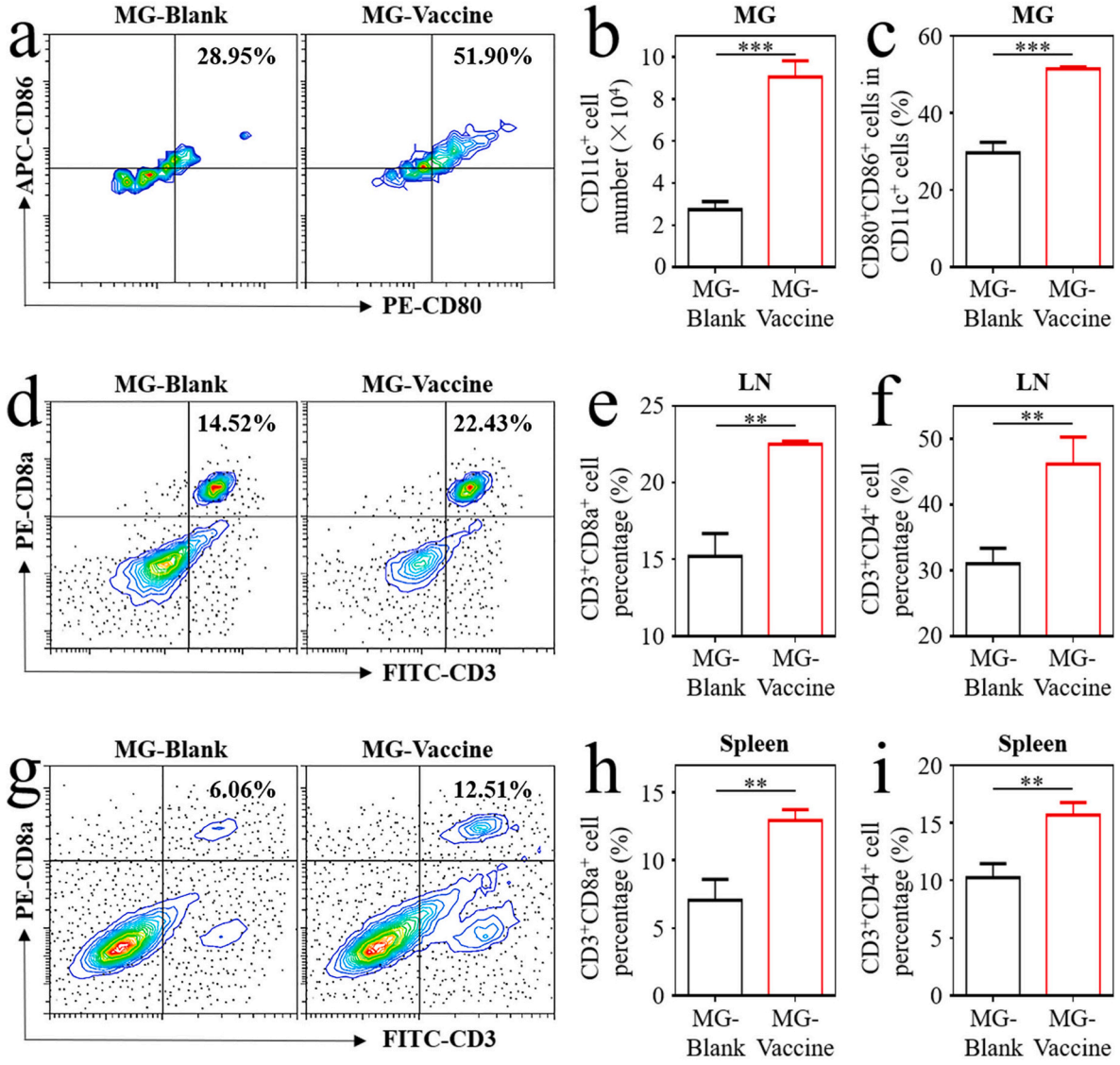

Fig. 4. *In vivo* immune response of the microgels. (a, c) (a) Representative flow cytometry data and (c) statistical data of $CD80^+CD86^+$ cells in $CD11c^+$ cells in the microgels on day 7 after injection of 200 μL MG-Blank or MG-Vaccine (n = 3). (b) $CD11c^+$ cell number in the microgels on day 7 after injection (n = 3). (d, e, f) (d) Representative flow cytometry data of $CD3^+CD8a^+$ cells, and statistical data of (e) $CD3^+CD8a^+$ cells and (f) $CD3^+CD4^+$ cells in the draining lymph node (LN) on day 7 after injection (n = 3). (g, h, i) (g) Representative flow cytometry data of $CD3^+CD8a^+$ cells, and statistical data of (h) $CD3^+CD8a^+$ cells and (i) $CD3^+CD4^+$ cells in the spleen on day 7 after injection (n = 3). Data are presented as mean ± SD. Statistical significance was calculated using Student's t-test. *$p < 0.05$, **$p < 0.01$, ***$p < 0.001$., ****$p < 0.0001$.

long-term survival of the mice in each group was also studied. MG-V+A group showed the longest survival, with two of the mice surviving more than 36 days (Fig. 5f). All the results indicated that the cryo-shocked cancer cell-loaded microgels hold prominent oncotherapy efficacy.

To explore the mechanisms behind the therapeutic effects generated by the microgel formulation, a tumor incomplete resection model was established. On day 7 after the operation, tumor-infiltrating lymphocytes were collected and then detected by flow cytometry. An increased frequency of both $CD8^+$ T cells and $CD4^+$ T cells was verified in the MG-V+A group (Fig. 5g and h, and Figs. S19 and S20). Such consequences illustrated that the blockade of the PD-1/PD-L1 pathway could effectively enhance the T-cell immunity induced by the microgel-based cancer vaccine. As a population of immunosuppressive cells, regulatory T cells (Tregs, $CD4^+$ $FoxP3^+$ cells) exert a major negative effect on the antitumor immune response. As shown in Fig. 5i and Fig. S21, the proportions of $FoxP3^+$ cells in $CD4^+$ cells in the MG-aPD1 group and MG-V+A group were significantly lower than that in the groups without aPD1, indicating that the application of aPD-1 could decrease the number of the Tregs to alleviate the tumor-induced immune suppression. The microgels encapsulating cryo-shocked cancer cells and immunoadjuvant could provoke the anti-tumor immune response, which was further enhanced by the immune checkpoint blockade.

3.5. *In vitro and in vivo tissue reconstruction properties of microgels*

After tumor resection, in addition to tumor recurrence/metastasis, loss of tissues is also a threat to the quality of life of patients. As a potential tissue regeneration platform, the microgels are supposed to have the ability to support the attachment and proliferation of normal tissue cells to achieve tissue repair. In theory, Arg-Gly-Asp (RGD) cell adhesion peptides of GelMA can promote cell adhesion, and the constitution of GelMA and HAMA, which are similar to ECM, can provide support for cell growth [36,39,43]. Therefore, the capability of the microgels for tissue regeneration was investigated.

To rule out interference from inactivated cancer cells, MG-Blank was used for *in vitro* and *in vivo* experiments. After the co-incubation of MCF-

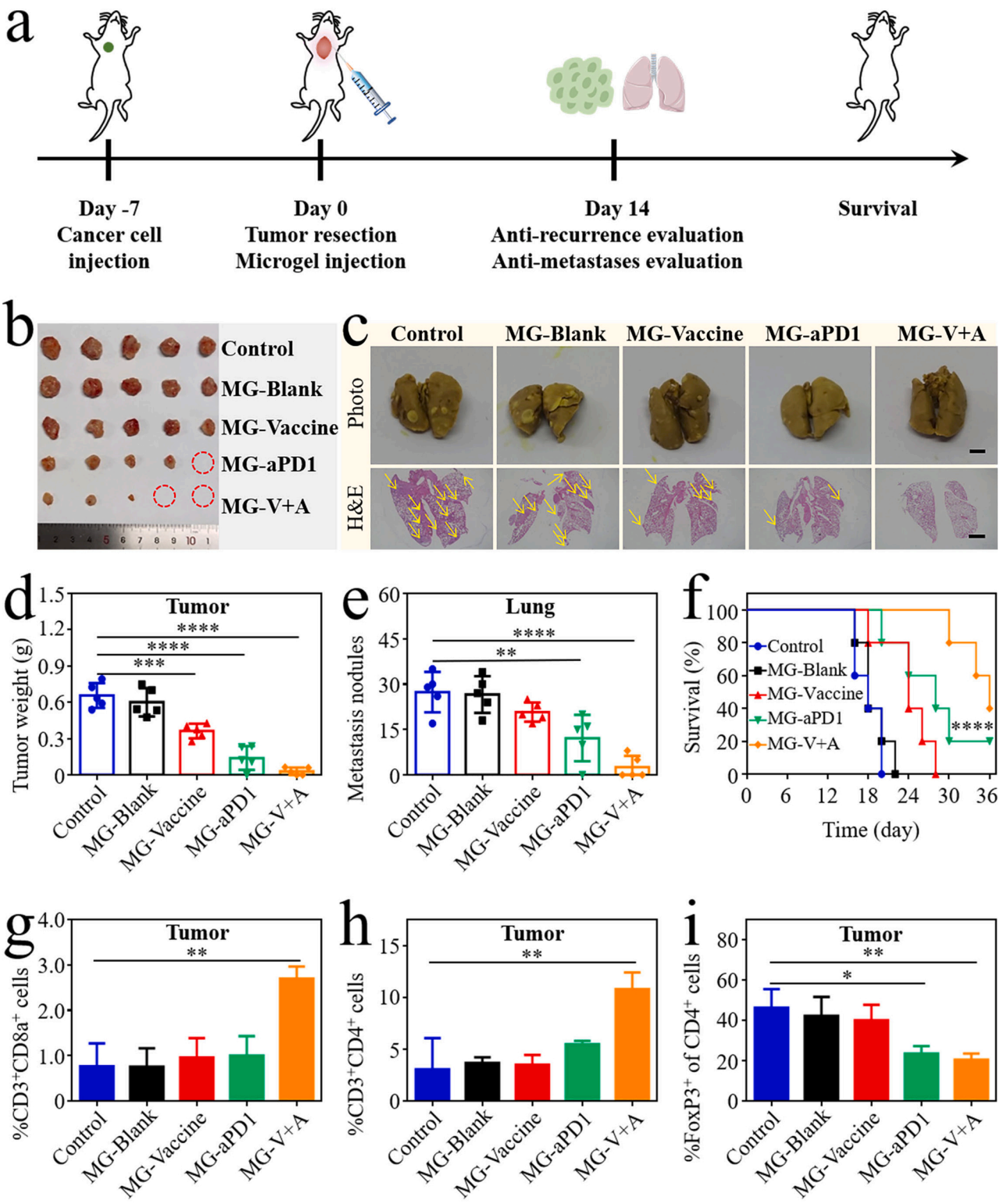

Fig. 5. *In vivo* anti-recurrence and anti-metastasis efficacy. (a) Diagram of breast tumor model establishment and treatment schedule. (b) Photographs of the recurrent tumors on day 14 after tumor resection and injection of 200 μL MG-Blank, MG-Vaccine, MG-aPD1, or MG-V+A. Mice without microgel injection were set as control. Red dotted circles indicate no tumor recurrence. (c) Representative photographs and H&E staining of lungs collected from mice on day 14 after the operation. White nodules and yellow arrows indicate lung metastases. Scale bars are 2 mm. (d) Weight of tumors on day 14 after the operation (n = 5). (e) The number of macroscopically visible metastases in the lungs on day 14 after the operation (n = 5). (f) The survival rate of mice with different treatments after the operation (n = 5). (g, h) Statistical data of (g) $CD3^+CD8a^+$ cells and (h) $CD3^+CD4^+$ cells in the tumors on day 7 after the tumor incomplete resection and injection of 200 μL MG-Blank, MG-Vaccine, MG-aPD1, or MG-V+A. Mice without microgel injection were set as control (n = 3). (i) Statistical data of $FoxP3^+$ cells in $CD4^+$ cells in the tumors on day 7 after the operation (n = 3). Statistical significance was calculated by one-way ANOVA using the Turkey post-hoc test or log-rank test (survival curves comparison). *$p < 0.05$, **$p < 0.01$, ***$p < 0.001$, ****$p < 0.0001$.

10A and ADSCs with MG-blank for 24 h, cell attachment on the microgels was confirmed by SEM (Fig. 6a). The proliferation of cells adhered to the microgels was then evaluated by Calcein AM staining and CCK8 assay. As shown in Fig. 6b, the number of cells with green fluorescence increased with time, indicating the proliferation of the cells adhered to the microgels. And the increasing absorbance tested by CCK8 assay also demonstrated that cells could continuously proliferate from day 0 to day 4 (Fig. 6c). Besides, adherent cells on the microgels showed a spreading morphology and covered the entire surface of the microgels on day 4 (Fig. S22). Furthermore, MG-Blank was injected subcutaneously into the mice and isolated for H&E staining. As shown in Fig. S23, compared with microgels on day 0, there were cells on the microgels on days 7 and 21, and the number of cells increased evidently with the extension of injection time. Collectively, these preliminary data provided evidence in the regeneration of normal tissue on the microgels.

Prevention of tumor recurrence/metastasis and tissue regeneration after surgery is vital for the long survival and high life quality of patients with cancer. Biomaterial scaffolds have attracted increasing attention and some remarkable results have been obtained in recent years [21, 44–46]. On the one hand, scaffolds such as electrospun fiber, hydrogel, and 3D printing scaffolds, can provide support for tissue cells. On the other hand, as drug delivery systems, they can be used for postoperative antitumor therapy by delivering chemotherapeutics or photothermal agents. In contrast to previous studies, the microgels in our study were not only a carrier of therapeutic components and support for tissue cell attachment and proliferation, but also a scaffold for recruited DC activation *in situ* to provoke an enhanced antitumor immune response (Fig. 4). In postoperative tumor models, the cryo-shocked cancer cell microgels exhibited a synergistic antitumor effect of the scaffold-based cancer vaccine and immune checkpoint inhibitor (Fig. 5). Apart from anti-recurrence/anti-metastases abilities, the tissue regeneration performance of the microgels was evaluated. According to Fig. 2f and **S17**, the cryo-shocked cancer cell microgels should be a favorable filler for dissected empty spaces after surgery. After the injection of the microgels, the cells were grown on the microgels, and the number of cells increased with time (Fig. S23). These results validate the potential use of microgels for anticancer treatment and tissue regeneration following surgical resection.

4. Conclusions

In summary, we have developed novel cryo-shocked cancer cell microgels with the desired multi-functions for post-surgical tumor treatment. Owing to the encapsulation of cryo-shocked cancer cells and immunoadjuvant, the microgels acted as a synthetic immune niche to initiate a potent immune response, which was further strengthened with the co-loading of immune checkpoint inhibitors. Based on this, we demonstrated that the cryo-shocked cancer cell microgels showed excellent anti-recurrence and anti-metastasis performances in the mouse breast cancer model. Besides, because of the excellent biocompatibility and suitable degradation rate, the microgels can provide support for normal cell adhesion and growth, thus serving as 3D scaffolds for tissue regeneration. These characteristics indicated the great potential of the cryo-shocked cancer cell microgels as a multifunctional platform for efficient postoperative cancer therapy.

Ethics approval and consent to participate

All experimental designs and protocols involving animals were approved by the Animal Ethics Committee of the Wenzhou Institute, University of Chinese Academy of Sciences (approval WIUCAS22080202) and complied with the recommendations of the academy's animal research guidelines.

CRediT authorship contribution statement

Gaizhen Kuang: Conceptualization, Methodology, Investigation, Data curation, Writing – original draft, Writing – review & editing, Funding acquisition. **Qingfei Zhang:** Methodology, Investigation, Formal analysis, Writing – original draft, Funding acquisition. **Yunru Yu:** Investigation, Writing – review & editing. **Luoran Shang:** Writing – review & editing, Supervision. **Yuanjin Zhao:** Conceptualization, Writing – review & editing, Supervision, Funding acquisition.

Declaration of competing interest

The authors declare that they have no known competing financial

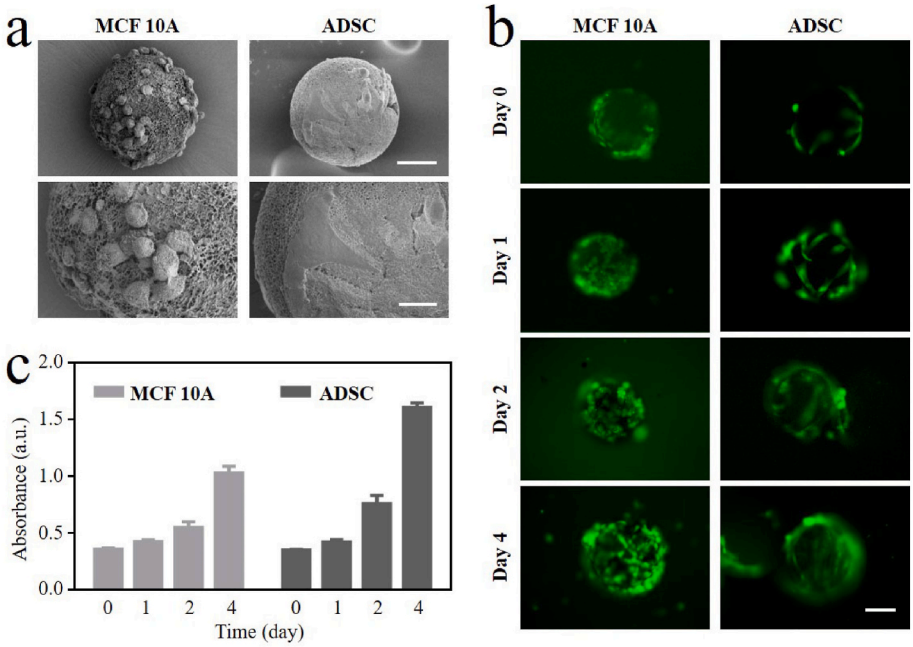

Fig. 6. *In vitro* tissue reconstruction property of the microgels. (a) SEM images of the blank microgels co-cultured with MCF 10A or ADSCs for 24 h. Scale bars are 50 μm in upper images and 20 μm in lower images. (b) Fluorescence images of Calcein AM stained MCF 10A or ADSCs adhered to the blank microgels on different days. Scale bar is 100 μm. (c) Cell proliferation analysis of MCF 10A or ADSCs adhered to the blank microgels by CCK8 assay (n = 4). Data are presented as mean ± SD.

interests or personal relationships that could have appeared to influence the work reported in this paper.

Acknowledgments

This work was supported by the National Key Research and Development Program of China (2020YFA0908200), the National Natural Science Foundation of China (32201118, 52073060, and 52103196), the Guangdong Basic and Applied Basic Research Foundation (2021B1515120054), and the Shenzhen Fundamental Research Program (JCYJ20190813152616459 and JCYJ20210324133214038).

Appendix A. Supplementary data

Supplementary data to this article can be found online at https://doi.org/10.1016/j.bioactmat.2023.05.021.

References

[1] H. Sung, J. Ferlay, R.L. Siegel, M. Laversanne, I. Soerjomataram, A. Jemal, F. Bray, Global cancer statistics 2020: GLOBOCAN estimates of incidence and mortality worldwide for 36 cancers in 185 countries, CA A Cancer J. Clin. 71 (3) (2021) 209–249.

[2] Z. Zhang, G. Kuang, S. Zong, S. Liu, H. Xiao, X. Chen, D. Zhou, Y. Huang, Sandwich-like fibers/sponge composite combining chemotherapy and hemostasis for efficient postoperative prevention of tumor recurrence and metastasis, Adv. Mater. 30 (49) (2018), e1803217.

[3] C. Feng, J. Ouyang, Z. Tang, N. Kong, Y. Liu, L. Fu, X. Ji, T. Xie, O.C. Farokhzad, W. Tao, Germanene-based theranostic materials for surgical adjuvant treatment: inhibiting tumor recurrence and wound infection, Matter 3 (1) (2020) 127–144.

[4] Q. Zhang, G. Kuang, S. He, S. Liu, H. Lu, X. Li, D. Zhou, Y. Huang, Chain-shattering Pt(IV)-backboned polymeric nanoplatform for efficient CRISPR/Cas9 gene editing to enhance synergistic cancer therapy, Nano Res. 14 (3) (2020) 601–610.

[5] G. Kuang, H. Lu, S. He, H. Xiong, J. Yu, Q. Zhang, Y. Huang, Near-infrared light-triggered polyprodrug/siRNA loaded upconversion nanoparticles for multi-modality imaging and synergistic cancer therapy, Adv. Healthc. Mater. 10 (20) (2021), e2100938.

[6] Q. Zhang, G. Kuang, S. He, H. Lu, Y. Cheng, D. Zhou, Y. Huang, Photoactivatable prodrug-backboned polymeric nanoparticles for efficient light-controlled gene delivery and synergistic treatment of platinum-resistant ovarian cancer, Nano Lett. 20 (5) (2020) 3039–3049.

[7] Q. Zhang, G. Kuang, D. Zhou, Y. Qi, M. Wang, X. Li, Y. Huang, Photoactivated polyprodrug nanoparticles for effective light-controlled Pt(iv) and siRNA codelivery to achieve synergistic cancer therapy, J. Mater. Chem. B 8 (27) (2020) 5903–5911.

[8] Q. Zhang, S. He, G. Kuang, S. Liu, H. Lu, X. Li, D. Zhou, Y. Huang, Morphology tunable and acid-sensitive dextran-doxorubicin conjugate assemblies for targeted cancer therapy, J. Mater. Chem. B 8 (31) (2020) 6898–6904.

[9] T. Sun, Y.S. Zhang, B. Pang, D.C. Hyun, M. Yang, Y. Xia, Engineered nanoparticles for drug delivery in cancer therapy, Angew Chem. Int. Ed. Engl. 53 (46) (2014) 12320–12364.

[10] Q. Zhang, X. Wang, G. Kuang, Y. Zhao, Pt(IV) prodrug initiated microparticles from microfluidics for tumor chemo-, photothermal and photodynamic combination therapy, Bioact. Mater. 24 (2023) 185–196.

[11] Y. Yang, Cancer immunotherapy: harnessing the immune system to battle cancer, J. Clin. Invest. 125 (9) (2015) 3335–3337.

[12] S.B. Stephan, A.M. Taber, I. Jileaeva, E.P. Pegues, C.L. Sentman, M.T. Stephan, Biopolymer implants enhance the efficacy of adoptive T-cell therapy, Nat. Biotechnol. 33 (1) (2015) 97–101.

[13] P. Yang, H. Song, Y. Qin, P. Huang, C. Zhang, D. Kong, W. Wang, Engineering dendritic-cell-based vaccines and PD-1 blockade in self-assembled peptide nanofibrous hydrogel to amplify antitumor T-cell immunity, Nano Lett. 18 (7) (2018) 4377–4385.

[14] H. Wang, J.A. Najibi, M.C. Sobral, B.R. Seo, J.Y. Lee, D. W, A.W. Li, C.S. Verbeke, D.J. Mooney, Biomaterial-based scaffold for in situ chemo-immunotherapy to treat poorly immunogenic tumors, Nat. Commun. 11 (1) (2020) 5696.

[15] Q. Chen, C. Wang, X. Zhang, G. Chen, Q. Hu, H. Li, J. Wang, D. Wen, Y. Zhang, Y. Lu, G. Yang, C. Jiang, J. Wang, G. Dotti, Z. Gu, In situ sprayed bioresponsive immunotherapeutic gel for post-surgical cancer treatment, Nat. Nanotechnol. 14 (1) (2019) 89–97.

[16] S. Han, J. Wu, Three-dimensional (3D) scaffolds as powerful weapons for tumor immunotherapy, Bioact, Materials 17 (2022) 300–319.

[17] J. Weiden, J. Tel, C.G. Figdor, Synthetic immune niches for cancer immunotherapy, Nat. Rev. Immunol. 18 (3) (2018) 212–219.

[18] G. Kuang, Q. Zhang, Y. Yu, X. Ding, W. Sun, X. Shen, Y. Zhao, Lyophilization-inactivated cancer cells composited Janus scaffold for tumor postoperative immuno-chemotherapy, Chem. Eng. J. 455 (2023), 140619.

[19] Y. Jun, E. Kang, S. Chae, S.H. Lee, Microfluidic spinning of micro- and nano-scale fibers for tissue engineering, Lab Chip 14 (13) (2014) 2145–2160.

[20] Z. Yang, D. Gao, X. Guo, L. Jin, J. Zheng, Y. Wang, S. Chen, X. Zheng, L. Zeng, M. Guo, X. Zhang, Z. Tian, Fighting immune cold and reprogramming immunosuppressive tumor microenvironment with red blood cell membrane-camouflaged nanobullets, ACS Nano 14 (12) (2020) 17442–17457.

[21] Y. Luo, X. Wei, Y. Wan, X. Lin, Z. Wang, P. Huang, 3D printing of hydrogel scaffolds for future application in photothermal therapy of breast cancer and tissue repair, Acta Biomater. 92 (2019) 37–47.

[22] Q. Zhang, X. Wang, G. Kuang, Y. Yu, Y. Zhao, Photopolymerized 3D printing scaffolds with Pt(IV) prodrug initiator for postsurgical tumor treatment, Research 2022 (2022), 9784510.

[23] T. Ci, H. Li, G. Chen, Z. Wang, J. Wang, P. Abdou, Y. Tu, G. Dotti, Z. Gu, Cryo-shocked cancer cells for targeted drug delivery and vaccination, Sci. Adv. 6 (50) (2020), eabc3013.

[24] J. Guo, H. De May, S. Franco, A. Noureddine, L. Tang, C.J. Brinker, D.F. Kusewitt, S.F. Adams, R.E. Serda, Cancer vaccines from cryogenically silicified tumour cells functionalized with pathogen-associated molecular patterns, Nat. Biomed. Eng. 6 (1) (2022) 19–31.

[25] Y. Wang, X. Zhang, L. Shang, Y. Zhao, Thriving microfluidic technology, Sci. Bull. 66 (1) (2021) 9–12.

[26] X. Hou, Y.S. Zhang, G.T. Santiago, M.M. Alvarez, J. Ribas, S.J. Jonas, P.S. Weiss, A. M. Andrews, J. Aizenberg, A. Khademhosseini, Interplay between materials and microfluidics, Nat. Rev. Mater. 2 (5) (2017) 1–15.

[27] D. Liu, H. Zhang, F. Fontana, J.T. Hirvonen, H.A. Santos, Current developments and applications of microfluidic technology toward clinical translation of nanomedicines, Adv. Drug Deliv. Rev. 128 (2018) 54–83.

[28] Z. Zhao, Z. Wang, G. Li, Z. Cai, J. Wu, L. Wang, L. Deng, M. Cai, W. Cui, Injectable microfluidic hydrogel microspheres for cell and drug delivery, Adv. Funct. Mater. 31 (31) (2021), 2103339.

[29] Q. Zhang, G. Kuang, Y. Yu, X. Ding, H. Ren, W. Sun, Y. Zhao, Hierarchical microparticles delivering oxaliplatin and NLG919 nanoprodrugs for local chemo-immunotherapy, ACS Appl. Mater. Interfaces 14 (43) (2022) 48527–48539.

[30] V. Vergaro, F. Scarlino, C. Bellomo, R. Rinaldi, D. Vergara, M. Maffia, F. Baldassarre, G. Giannelli, X. Zhang, Y.M. Lvov, S. Leporatti, Drug-loaded polyelectrolyte microcapsules for sustained targeting of cancer cells, Adv. Drug Deliv. Rev. 63 (9) (2011) 847–864.

[31] J. Pessi, H.A. Santos, I. Miroshnyk, Jouko Yliruusi, D.A. Weitz, S. Mirza, Microfluidics-assisted engineering of polymeric microcapsules with high encapsulation efficiency for protein drug delivery, Int. J. Pharm. 472 (1–2) (2014) 82–87.

[32] D. Liu, H. Zhang, F. Fontana, J.T. Hirvonen, H.A. Santos, Microfluidic-assisted fabrication of carriers for controlled drug delivery, Lab Chip 17 (11) (2017) 1856–1883.

[33] A.C. Daly, L. Riley, T. Segura, J.A. Burdick, Hydrogel microparticles for biomedical applications, Nat. Rev. Mater. 5 (1) (2020) 20–43.

[34] J. Hao, B. Bai, Z. Ci, J. Tang, G. Hu, C. Dai, M. Yu, M. Li, W. Zhang, Y. Zhang, W. Ren, Y. Hua, G. Zhou, Large-sized bone defect repair by combining a decalcified bone matrix framework and bone regeneration units based on photo-crosslinkable osteogenic microgels, Bioact. Mater. 14 (2022) 97–109.

[35] Z. Zhao, G. Li, H. Ruan, K. Chen, Z. Cai, G. Lu, R. Li, L. Deng, M. Cai, W. Cui, Capturing magnesium ions via microfluidic hydrogel microspheres for promoting cancellous bone regeneration, ACS Nano 15 (8) (2021) 13041–13054.

[36] Y. Lei, Y. Wang, J. Shen, Z. Cai, Y. Zeng, P. Zhao, J. Liao, C. Lian, N. Hu, X. Luo, W. Cui, W. Huang, Stem cell-recruiting injectable microgels for repairing osteoarthritis, Adv. Funct. Mater. 31 (48) (2021), 2105084.

[37] X. Zhao, S. Liu, L. Yildirimer, H. Zhao, R. Ding, H. Wang, W. Cui, D. Weitz, Injectable stem cell-laden photocrosslinkable microspheres fabricated using microfluidics for rapid generation of osteogenic tissue constructs, Adv. Funct. Mater. 26 (17) (2016) 2809–2819.

[38] J. Antunes, V.M. Gaspar, L. Ferreira, M. Monteiro, R. Henrique, C. Jeronimo, J. F. Mano, In-air production of 3D co-culture tumor spheroid hydrogels for expedited drug screening, Acta Biomater. 94 (2019) 392–409.

[39] A.G. Kurian, R.K. Singh, K.D. Patel, J.H. Lee, H.W. Kim, Multifunctional GelMA platforms with nanomaterials for advanced tissue therapeutics, Bioact. Mater. 8 (2022) 267–295.

[40] D.M. Klinman, Immunotherapeutic uses of CpG oligodeoxynucleotides, Nat. Rev. Immunol. 4 (4) (2004) 249–258.

[41] A.A. Omar, H. Nathaniel, C. Lan, D. Glenn, J.M. David, Infection-mimicking materials to program dendritic cells in situ, Nat. Mater. 8 (2) (2009) 151–158.

[42] H. Song, P. Huang, J. Niu, G. Shi, C. Zhang, D. Kong, W. Wang, Injectable polypeptide hydrogel for dual-delivery of antigen and TLR3 agonist to modulate dendritic cells in vivo and enhance potent cytotoxic T-lymphocyte response against melanoma, Biomaterials 159 (2018) 119–129.

[43] Y.H. Ahn, L. Ren, S.M. Kim, S.H. Seo, C.R. Jung, D.S. Kim, J.Y. Noh, S.Y. Lee, H. Lee, M.Y. Cho, H. Jung, S.R. Yoon, J.E. Kim, S.N. Lee, S. Kim, I.W. Shin, H. S. Shin, K.S. Hong, Y.T. Lim, I. Choi, T.D. Kim, A three-dimensional hyaluronic acid-based niche enhances the therapeutic efficacy of human natural killer cell-based cancer immunotherapy, Biomaterials 247 (2020), 119960.

[44] X. Liu, H. Zhang, R. Cheng, Y. Gu, Y. Yin, Z. Sun, G. Pan, Z. Deng, H. Yang, L. Deng, W. Cui, H.A. Santos, Q. Shi, An immunological electrospun scaffold for tumor cell killing and healthy tissue regeneration, Mater. Horiz. 5 (6) (2018) 1082–1091.
[45] J.D. Obayemi, S.M. Jusu, A.A. Salifu, S. Ghahremani, M. Tadesse, V.O. Uzonwanne, W.O. Soboyejo, Degradable porous drug-loaded polymer scaffolds for localized cancer drug delivery and breast cell/tissue growth, Mater. Sci. Eng. C Mater. Biol. Appl. 112 (2020), 110794.
[46] X. Yang, L. Gao, Y. Wei, B. Tan, Y. Wu, C. Yi, J. Liao, Photothermal hydrogel platform for prevention of post-surgical tumor recurrence and improving breast reconstruction, J. Nanobiotechnol. 19 (1) (2021) 1–13.